Voltage-gated proton channels maintain pH in human neutrophils during phagocytosis

Deri Morgan[a], Melania Capasso[b], Boris Musset[a], Vladimir V. Cherny[a], Eduardo Ríos[a], Martin J. S. Dyer[b], and Thomas E. DeCoursey[a,1]

[a]Department of Molecular Biophysics and Physiology, Rush University Medical Center, Chicago, IL 60612; and [b]Medical Research Council Toxicology Unit, University of Leicester, Leicester LE1 9HN, United Kingdom

Phagocytosis of microbial invaders represents a fundamental defense mechanism of the innate immune system. The subsequent killing of microbes is initiated by the respiratory burst, in which nicotinamide adenine dinucleotide phosphate (NADPH) oxidase generates vast amounts of superoxide anion, precursor to bactericidal reactive oxygen species. Cytoplasmic pH regulation is crucial because NADPH oxidase functions optimally at neutral pH, yet produces enormous quantities of protons. We monitored pH_i in individual human neutrophils during phagocytosis of opsonized zymosan, using confocal imaging of the pH sensing dye SNARF-1, enhanced by shifted excitation and emission ratioing, or SEER. Despite long-standing dogma that Na^+/H^+ antiport regulates pH during the phagocyte respiratory burst, we show here that voltage-gated proton channels are the first transporter to respond. During the initial phagocytotic event, pH_i decreased sharply, and recovery required both Na^+/H^+ antiport and proton current. Inhibiting myeloperoxidase attenuated the acidification, suggesting that diffusion of HOCl into the cytosol comprises a substantial acid load. Inhibiting proton channels with Zn^{2+} resulted in profound acidification to levels that inhibit NADPH oxidase. The pH changes accompanying phagocytosis in bone marrow phagocytes from HVCN1-deficient mice mirrored those in control mouse cells treated with Zn^{2+}. Both the rate and extent of acidification in HVCN1-deficient cells were twice larger than in control cells. In summary, acid extrusion by proton channels is essential to the production of reactive oxygen species during phagocytosis.

innate immunity | ion channels | phagocyte | respiratory burst | SNARF

We have reinvestigated the regulation of cytoplasmic pH, pH_i, in human neutrophils during phagocytosis. For 3 decades, pH_i during the respiratory burst has been characterized as a small (0.05–0.1 unit) transient drop in pH_i that is followed by larger (0.16–0.60 unit) prolonged alkalinization caused by Na^+/H^+ antiport activity, whether the stimulus is fMLF (fMetLeuPhe, a chemotactic peptide), PMA (a PKC-activating phorbol ester), phospholipase C, or OPZ (opsonized zymosan) (1–7). In most studies, soluble stimuli were applied to populations of neutrophils. When phagocytosis was studied, the responses of many cells were averaged (5, 8). A powerful new imaging approach, confocal microscopy using the fluorescent pH indicator SNARF-1 enhanced by shifted excitation and emission ratioing (SEER) (9, 10) enabled us to examine the responses of individual cells with high spatial and temporal resolution. We report here that the behavior of individual human neutrophils during phagocytosis differs markedly from the prevailing view. The fundamental pH_i response is triphasic: rapid and profound acidification followed by rapid but variably complete recovery, and after longer times, slow acidification that may reflect the onset of apoptosis.

Results

Cells That Phagocytose Become Acidic. Human neutrophils were allowed to adhere to a glass chamber at room temperature before opsonized zymosan (OPZ) was added. Neutrophils that adhere to substrate and spread are activated in the sense that NADPH oxidase is demonstrably active (11). Our measurements confirm that cells that strongly adhered to the glass substrate and were visibly spread at the outset of experiments tended to be acidic (pH_i 6.73 ± 0.09, mean ± SE, 28 cells from 3 experiments), whereas spherical cells had higher pH_i (7.11 ± 0.03, 30 cells from 3 experiments; $P < 0.001$). A field of cells was selected, and pH_i was monitored before and after addition of OPZ. Identifying cells containing OPZ was straightforward (Fig. 1A) and allowed us to retrospectively reconstruct the time course of pH_i of individual cells during phagocytosis. Cells that phagocytosed OPZ acidified on average over 60 min (Fig. 1 E and F). In contrast, cells that did not engulf OPZ tended to alkalinize moderately at low OPZ concentration (Fig. 1E). The fraction of phagocytosing cells increased with OPZ concentration: 10% with 0.1 mg/mL OPZ, 35% with 1 mg/mL OPZ, and 50% with 2 mg/mL OPZ, measured after 60 min. We routinely used 1–2 mg/mL OPZ to ensure a large fraction of phagocytosing cells. Neutrophils pretreated with the NADPH oxidase inhibitor diphenylene iodonium (DPI) did not acidify (Fig. 1 D and G) despite the same fraction phagocytosing (34% with 1 mg/mL OPZ), confirming that NADPH oxidase activity was the source of the acidification. Because pH_i tended to increase in nonphagocytosing cells, when the responses of all cells are averaged (as was done in previous population studies), pH_i increased at 0.1 or 0.5 mg/mL OPZ.

Rapid Acidification Coincides with the Initial Phagocytotic Event. The pH_i response of 4 individual neutrophils during phagocytosis is plotted in Fig. 2. Movies S1–S6 of representative cell responses are available in SI. Although the time course varied widely among cells, several consistent features emerged. Typically, pH_i did not change until phagocytosis began. Simultaneous with engulfment of OPZ, there was invariably a large rapid drop in pH_i that reached 0.35 ± 0.17 pH units (SD, $n = 200$) below the previous value. In cells exhibiting recovery, the nadir occurred after 3.4 ± 2.0 min (SD, $n = 58$). The large decrease in pH_i in phagocytosing neutrophils was unexpected and greatly exceeds reported responses (1, 3–5, 7). This apparent discrepancy is likely attributable mainly to the smearing of time courses of individual cells by averaging, inclusion of nonresponding cells, and use of soluble stimuli in previous studies. Recovery was rapid and sometimes complete (Fig. 2A), but rarely overshot the initial pH_i, and in other cells was incomplete or absent (Fig. 2B). In a sample of 96 phagocytosing cells categorized according to the extent of recovery, pH_i recovery was nearly complete in 34%,

Fig. 1. Only neutrophils that phagocytosed OPZ acidified. (*A*) Raw images at the 2 wavelengths ratioed for SEER (10), illustrating that cells that phagocytose OPZ (*Right*) can be readily distinguished. Human neutrophils were exposed to 0.5 mg/mL OPZ (*B*), 2 mg/mL OPZ (*C*), or 2 mg/mL OPZ with 20 μM DPI (*D*) at 0 min, and pH$_i$ was monitored in individual cells by SEER (10). (*E*) Mean ($\pm$ SE) pH$_i$ decreased in 35 cells that phagocytosed in 0.5 mg/mL OPZ ($\square$), whereas pH$_i$ increased in 43 cells that did not ($\blacksquare$). (*F*) At 2.0 mg/mL OPZ, 41 phagocytosing cells acidified; the apparent decline in pH$_i$ in 29 nonphagocytosing cells may reflect a few miscategorized cells that engulfed OPZ surreptitiously, outside the plane of focus. (*G*) Despite a normal rate of phagocytosis (see text), no acidification occurred when the NADPH oxidase was inhibited by 20 μM DPI ($\blacksquare$, 31 cells; $\square$, 34 cells).

partial in 36%, and absent in 28%. In cells exhibiting full recovery, the peak rate of pH$_i$ increase was 0.077 $\pm$ 0.008 units/min (mean $\pm$ SE, $n = 43$), approximately half as rapid as the onset of acidification.

By 10 min after phagocytosis, neutrophils typically exhibited a slow phase of acidification (e.g., Fig. 2*A*) that in most cells did not reverse by 1 h. Neutrophils do not survive very long ex vivo or after a respiratory burst. Within 3 h in culture, a fraction of (unstimulated) neutrophils spontaneously acidify to pH$_i$ $\approx$6.2 before apoptosis (12). The slow acidification observed in most cells that phagocytosed OPZ may reflect the onset of apoptosis accelerated by phagocytosis, as suggested by Coakley et al. (8).

Both Na⁺/H⁺ Antiport and Proton Channels Are Required for pH$_i$ Recovery. We assessed pharmacologically the contributions to pH$_i$ recovery of 3 main acid extrusion mechanisms of neutrophils. The V-type H⁺-ATPase was inhibited by 500 nM bafilo-

Fig. 2. Time course of pH$_i$ changes in 4 phagocytosing neutrophils. Pseudo-color images of each cell are positioned near the corresponding time point. The spatially averaged pH$_i$ of the cell is plotted, including only areas of cytoplasm above a threshold level of fluorescence intensity; areas below the cutoff (e.g., in phagosomes) are blanked. Acidification invariably occurred rapidly after productive contact with OPZ, often followed by rapid recovery (*A*), but sometimes not (*B*). In cells pretreated with 20 μM DMA to inhibit Na⁺/H⁺ antiport (*C*), or 100 μM Zn²⁺ to inhibit proton current (*D*), pH$_i$ decreased farther and did not recover.

mycin (Baf), Na⁺/H⁺ antiport was inhibited by 20 μM dimethylamiloride (DMA), and proton channels were inhibited by 100 μM ZnCl₂. In the presence of either DMA (Fig. 2*C*) or Zn²⁺ (Fig. 2*D*), there was little or no recovery of pH$_i$ in any cell studied (Movie S4 and Movie S6). This paradoxical finding suggests that neither transporter alone can restore pH$_i$ after phagocytosis.

In Fig. 3*A*, neutrophil pH$_i$ responses are averaged after synchronization according to the time at which pH$_i$ began to decrease in association with the first productive encounter with OPZ. The mean pH$_i$ in 41 control cells $\approx$14 min after OPZ phagocytosis was 6.68 $\pm$ 0.03 (SE). In the presence of Baf, there was slow, subtle additional acidification to 6.54 $\pm$ 0.05 ($n = 21$, $P = 0.015$), suggesting a minor and belated contribution of H⁺-ATPase to pH$_i$ regulation during phagocytosis. A similarly weak effect of Baf on pH$_i$ was reported in neutrophils phagocytosing bacteria (8). Inhibiting either Na⁺/H⁺ antiport or proton channels resulted in profound monotonic acidification to 6.14 $\pm$ 0.06 in DMA ($n = 30$) or 5.87 $\pm$ 0.07 in Zn²⁺ ($n = 43$) ($P < 0.0001$ for each).

The effects of Zn²⁺ on pH$_i$ were steeply concentration dependent (Fig. 3*C*). Although 30 μM Zn²⁺ had small effects, maximal acidification occurred in the presence of 100 μM Zn²⁺ with no further acidification by 300 μM or 1 mM Zn²⁺. Phago-

PHYSIOLOGY

Fig. 3. Temporal involvement of proton transporters during phagocytosis. (*A*) Average time course of pH$_i$ changes in individual phagocytosing neutrophils, retrospectively synchronized to the time they first engulfed OPZ (set at 1.5 min). Mean ± SE in 52 control cells (■), cells pretreated with 500 nM Baf (◇, $n = 22$), 20 μM DMA (○, $n = 39$), or 100 μM Zn^{2+} (▲, $n = 52$). (*B*) Maximum rate of pH change during the rapid acidification accompanying phagocytosis in neutrophils pretreated with 100 μM Zn^{2+}, 20 μM DMA, or 500 nM Baf. The rate determined from the steepest slope in each cell is plotted (mean ± SE) for 129 control, 50 Zn^{2+} ($P < 0.0001$), 39 DMA, 39 Baf, and 12 Zn^{2+}+DMA treated cells. (*C*) Concentration-dependent effects of Zn^{2+} on pH$_i$. Average time course of pH$_i$ changes in synchronized phagocytosing neutrophils in the presence of 0 (●, 52 cells), 30 (○, 38 cells), 100 (▲, 52 cells), 300 μM Zn^{2+} (□, 42 cells), or 1 mM Zn^{2+} (◇, 52 cells). Error bars are omitted for clarity; data at 100 μM, 300 μM, or 1 mM Zn^{2+} all differed significantly from control, but not from each other. The data at 0 and 100 μM Zn^{2+} are the same as in (*A*).

cytosis was inhibited reversibly by high Zn^{2+} concentrations. The mean number of phagosomes visible in a confocal slice of each cell 30 min after OPZ addition was 3.48 ± 0.11 in 181 control cells, 1.87 ± 0.15 in 69 cells with 300 μM Zn^{2+}, and 0.63 ± 0.12 in 38 cells with 3 mM Zn^{2+} ($P < 0.001$).

Proton Channel Is the First to Respond. Alone among the inhibitors studied, Zn^{2+} altered the maximum rate of acidification during the initial phagocytic event (Fig. 3*B*), doubling it from 0.16 to 0.31 pH units min^{-1}. No further increase was observed when DMA was added together with Zn^{2+}. The acceleration of acidification by Zn^{2+} indicates that the proton channel is the first acid-extrusion mechanism to turn on during phagocytosis. This conclusion is generally consistent with the observations of Coakley et al. (8) that in populations of neutrophils phagocytosing bacteria, ZnCl$_2$ decreased pH$_i$ significantly during the first 20 min, whereas effects of amiloride occurred at 10–60 min.

The initial pH$_i$ varied, but had negligible effect on the magnitude or the extent of rapid acidification ($R^2 = 0.041$). In some cells, pH$_i$ decreased upon addition of either DMA or Zn^{2+}. We interpret this to mean that these cells were already "activated" by adherence (11). However, many cells exhibited no pH change with either inhibitor; we conclude that these cells were resting. We excluded from further analysis cells that acidified distinctly upon addition of Zn^{2+} or DMA.

HOCl Diffusion from the Phagosome Contributes to Cytoplasmic Acidification. Roughly half of the O$_2^{\cdot-}$ generated by NADPH oxidase during the respiratory burst of phagocytosis is converted to HOCl by myeloperoxidase (MPO) (13–17). We therefore inhibited MPO by including 500 μM ABAH (4-aminobenzoic acid hydrazide) in the medium (18). ABAH consistently reduced the extent of acidification in averaged responses of cells retrospectively synchronized (Fig. 4*A*). Measured 20 min after phagocytosis, pH$_i$ in control cells decreased by −0.48 ± 0.02 units (mean ± SEM, $n = 35$) compared with −0.19 ± 0.03 units ($n = 34$) in ABAH-treated cells ($P < 0.0001$). Similar findings were obtained using 10 mM sodium azide, which also inhibits MPO, but less selectively than ABAH. The simplest interpretation is that HOCl produced in the phagosome diffuses across the membrane into the cytosol, lowering pH$_i$. In the presence of both ABAH and 200 μM Zn^{2+}, there was profound acidification, roughly comparable to that observed in the presence of Zn^{2+} alone (cf. Fig. 3*A*).

ABAH did not affect the maximum rate of acidification (Fig. 4*B*), but in the presence of ABAH, Zn^{2+} doubled the rate from 0.16 to 0.33 pH units/min, identical to corresponding rates in the absence of ABAH (Fig. 3*B*). Effects of ABAH first became evident ≈10 min after the onset of phagocytosis, consistent with gradual accumulation of protons in the cytoplasm.

Responses of HVCN1-Deficient Mouse Bone Marrow Phagocytes Support the Proposed Role of Proton Channels. Because Zn^{2+} does not selectively inhibit proton channels, mice deficient in the HVCN1 proton channel were studied. Proton channel "knockout" (KO) mouse bone marrow cells have no detectable proton current, either before or after PMA stimulation (Fig. 5*A*), but they do exhibit electron current that reflects NADPH oxidase activity, confirmed by DPI inhibition (Fig. 5*B*). Fig. 5*C* illustrates proton currents in a WT mouse cell, and their response to PMA. As in human neutrophils (19, 20), proton channel gating is greatly enhanced over several minutes, and an inward electron current appears (Fig. 5*D*). No significant difference in electron current amplitude was detected in WT (−1.20 ± 0.28 pA, mean ± SEM, $n = 9$) and KO (−0.93 ± 0.28 pA, $n = 4$) bone marrow cells ($P = 0.56$). Bone
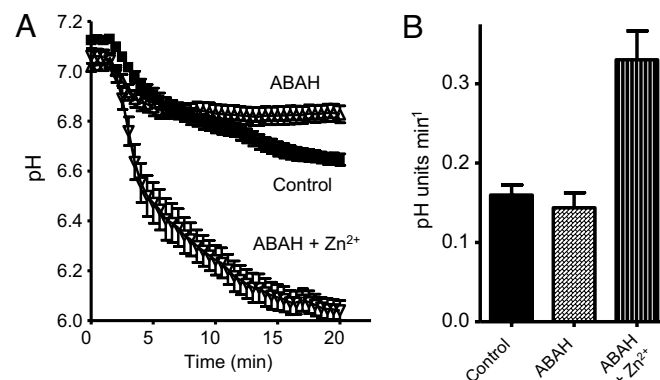
Fig. 4. Inhibition of MPO attenuates cytosolic acidification during phagocytosis. (*A*) Time course of pH$_i$ in phagocytosing neutrophils synchronized as in Fig. 3*A*, in 36 control cells (■), 35 cells in the presence of 500 μM ABAH, and 18 cells treated with 500 μM ABAH and 200 μM ZnCl$_2$, each in 3 separate experiments. (*B*) The maximum rate of acidification in the cells depicted in (*A*) was not changed by ABAH ($P = 0.48$), but increased significantly in the presence of ABAH and 200 μM Zn^{2+} ($P < 0.0001$).
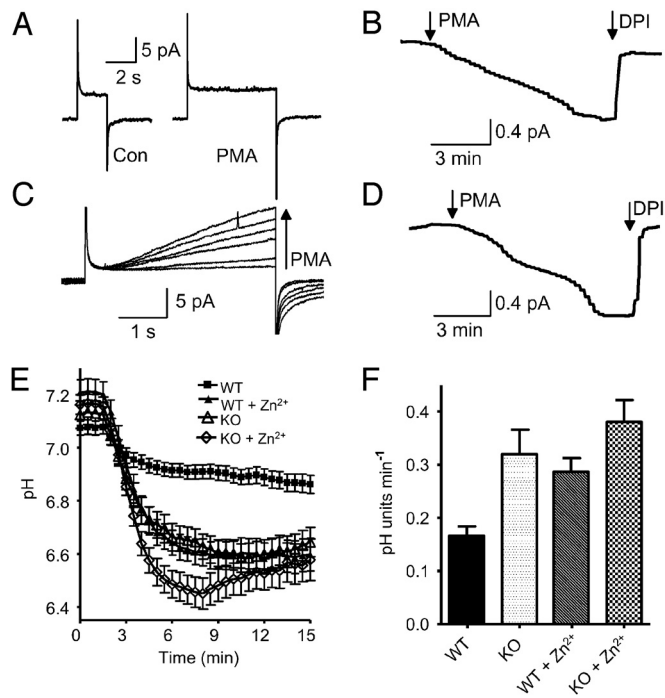
Fig. 5. Responses to OPZ of bone marrow phagocytes from WT and HVCN1 deficient (KO) mice. (*A*) Phagocytes from KO mice have no proton current. Currents are for pulses to +100 mV before (*Left*) and after (*Right*) 150 nM PMA. (*B*) Electron current elicited by PMA in the same cell at +20 mV, showing inhibition by 20 μM DPI, an NADPH oxidase inhibitor. (*C*) PMA response of WT proton currents during pulses to +80 mV applied at 1-min intervals before and after PMA. (*D*) Electron current elicited by PMA at −40 mV in the same cell. (*E*) Average time course of pH$_i$ in mouse bone marrow phagocytes exposed to OPZ. Each cell was retrospectively synchronized so the first phagocytic event occurred at 1.5 min. Measurements in cells from 3 different mice are combined for each condition. Mean ± SEM is plotted for 32 WT cells (■), 21 WT cells with 100 μM Zn^{2+} (▲), 23 KO cells (△), and 18 KO cells with 100 μM Zn^{2+} (◇). At 6 min, KO, KO+Zn^{2+}, and WT+Zn^{2+} all differ significantly from control (*P* < 0.01), but not from each other, with the exception that KO+Zn^{2+} differs from KO (*P* < 0.05). (*F*) Maximum rate of pH$_i$ decrease during the initial phagocytotic event in mouse bone marrow phagocytes. Mean ± SEM is plotted for 34 WT cells, 22 WT cells with 100 μM Zn^{2+}, 24 KO cells, and 18 KO cells with 100 μM Zn^{2+}. All data differ from WT (*P* < 0.001), but not from each other.

marrow cells are heterogeneous and not all responded to PMA, but some non-responses can be ascribed to spontaneous patch rupture. In most cells with a proton channel response, electron current was detected.

Fig. 5*E* illustrates that pH$_i$ changes during phagocytosis in mouse phagocytes resemble those in human neutrophils. The time course varied in individual WT mouse cells, with most cells acidifying upon phagocytosis and some exhibiting transient acidification (a spike). As in human cells, 100 μM Zn^{2+} enhanced the acidification. Importantly, the acidification was substantially greater in KO than in WT mouse phagocytes and closely resembled the time course in WT cells treated with Zn^{2+}. This finding suggests that Zn^{2+} affects pH$_i$ mainly by inhibiting proton channels. The depth of acidification in KO cells was somewhat greater in the presence of Zn^{2+}, a marginally significant difference that may reflect a small contribution from another Zn^{2+}-sensitive transporter.

Intriguingly, the peak rate of acidification in phagocytosing cells (Fig. 5*F*) was doubled by 100 μM Zn^{2+} and was also twice that of normal in KO cells, strongly implicating proton channels as responsible for the Zn^{2+} effect. Thus, as in human neutrophils, proton channels in mice appear to be active at the very outset of phagocytosis. Zn^{2+} did not significantly increase the acidifica-

tion rate in KO cells, indicating that no other Zn^{2+}-sensitive transporter is detectably active during the early pH$_i$ response.

Discussion

A Spike of Acidification Is Associated with Phagocytosis. Observation of the pH$_i$ of individual phagocytosing human neutrophils revealed that rapid acidification of 0.35 pH units occurred when the first zymosan particle was engulfed. In most cells, partial or complete recovery ensued. Proton channels, but not H$^+$-ATPase or Na$^+$/H$^+$ antiport, were demonstrably active during this early acidification phase (Figs. 3*B*, 4*B*, and 5*F*). Conventional wisdom postulates a shift in the set point of Na$^+$/H$^+$ antiport during the respiratory burst that results in sustained alkalinization (1–7). Three factors contribute to the apparent difference between our findings and those of previous investigations. First, we studied individual cells positively identified as phagocytosing, rather than mixed populations; Fig. 1*E* shows that the responses of phagocytosing and nonphagocytosing cells are qualitatively different. Second, the responses to OPZ and soluble stimuli likely differ. Finally, recovery from acidification required both Na$^+$/H$^+$ antiport and proton channels; previous studies simply reported acidification after inhibition of Na$^+$/H$^+$ antiport (as in Fig. 2*C*). Although H$^+$-ATPase activity was detected in neutrophils stimulated with fMLF (21), which does not elicit phagocytosis, H$^+$-ATPase activity was scarcely detectable during OPZ phagocytosis (Fig. 3*A*). The predominant regulator of pH$_i$ in phagocytosing neutrophils is the voltage-gated proton channel. Teleologically, this is reasonable, because the capacity for proton extrusion by proton channels exceeds that of other proton transporters by an order of magnitude, and unlike the H$^+$-ATPase and Na$^+$/H$^+$ antiport, the proton channel extrudes excess protons at no metabolic cost to the cell (22).

Although the rapid recovery of pH$_i$ certainly reflects H$^+$ extrusion, a decrease in NADPH oxidase activity may also contribute (23). Measurements of H$_2$O$_2$ in phagosomes from neutrophil-like PLB-985 cells indicate that NADPH oxidase activity begins before the phagosome is fully closed, increases rapidly for a few minutes, and then declines precipitously (24). The rapid recovery of pH$_i$ may thus reflect a combination of H$^+$ transport and cessation of NADPH oxidase activity.

HOCl Contributes to Cytosolic Acidification. It is clear that NADPH oxidase is the primary source of acid during the respiratory burst associated with phagocytosis in human neutrophils because DPI prevented any decrease in pH$_i$ (Fig. 1 *D* and *G*). The oxidation of NADPH releases one proton into the cytoplasm, and regeneration of NADPH produces a second proton via the hexose monophosphate shunt. If each electron translocated into the phagosome by NADPH oxidase were accompanied by one proton, via either proton channels or H-ATPase, there should be no net pH change in cytosol or phagosome (17, 25). Here, we show that distinct cytosolic acidification accompanies phagocytosis, followed by a tendency to recover. Most likely, the initial acidification reflects protons generated by NADPH oxidation and regeneration. At later times, however, the pH$_i$ decrease was attenuated by ABAH (Fig. 4), suggesting that HOCl produced in the phagosome diffuses into the cytosol and contributes significantly to the acid load. Previous demonstration that neutrophil proteins are chlorinated extensively supports this interpretation (16). In addition, a large fraction of the O$_2^{·−}$ produced by neutrophils is converted into HOCl (13–17). For ≈4 M electrons introduced cumulatively into the phagosome over a few minutes (25) at a rate of 5–20 mM s^{-1} (26, 27), ≈1 M Cl$^-$ is consumed to produce HOCl (17). The bulk of this Cl$^-$ must come from the cytoplasm. That Cl$^-$ is efficiently transported into the phagosome is supported by reversible changes of phagosomal Cl$^-$ in parallel with changes in bath Cl$^-$ concentration in neutrophils exposed to OPZ (28). Another electrogenic trans-

PHYSIOLOGY

porter may contribute to charge compensation, such as ClC-3, which is present in phagosomes in human neutrophils (29). However, when operating in the charge-compensation direction (H^+ into the phagosome, Cl^- out), ClC-3 would deplete the phagosome of Cl^-.

Without Proton Channels, Low pH_i Would Inhibit NADPH Oxidase. In the presence of 100 μM Zn^{2+}, pH_i in human neutrophils dropped to 6.5 two minutes after phagocytosis and to 6.0 after 10 min (Fig. 3A). Based on measurements in which pH_i was clamped by an NH_4^+ gradient, NADPH oxidase activity is inhibited at these pH_i by ≈50% and 80%, respectively (30). NADPH oxidase activity in proton channel knockout mouse leukocytes is attenuated by up to 75% (31–33). Much of this deficit can be attributed to the rapid drop in pH_i to 6.6 (Fig. 5A). Thus, despite the importance of charge compensation by proton channels (17, 20, 34–36), their role in preventing excessively low pH_i may be equally important for sustaining NADPH oxidase activity. Proton efflux uniquely performs both functions simultaneously.

The electron current is −2.3 pA in human neutrophils stimulated with phorbol myristate acetate (PMA) in perforated-patch voltage clamp at pH 7 and 20 °C (19). Assuming that one proton is generated in the cytoplasm for each electron translocated by NADPH oxidase (37, 38), a cell volume of 320 fL, and a cytoplasmic buffer capacity of 30 mM (3), pH_i would decrease by 0.27 units/min in the absence of proton extrusion. The peak rate of acidification in the presence of Zn^{2+} is 0.31–0.33 units/min (Figs. 3B and 4B), in excellent agreement with this value. Together with the prevention of acidification by DPI, these considerations indicate that NADPH oxidase activity during phagocytosis of OPZ generates acid in the cytoplasmic compartment at a rate consistent with complete charge separation across the phagosomal membrane.

Electron currents in KO bone marrow cells were of similar magnitude to WT cells. Because both pH_i and voltage were controlled during these measurements, the electron currents simply confirm the presence of normal NADPH oxidase. Despite the importance of pH and charge compensation by proton channels, some NADPH oxidase activity persists in HVCN1 KO mouse phagocytes (31–33), and in COS^{phox} cells that lack proton current (39), showing that charge compensation can occur independently of proton channels. The absence of proton current in HVCN1 KO mouse phagocytes exhibiting distinct electron current resolves conclusively the long-standing debate about whether the gp91^{phox} component of the active NADPH oxidase complex is a proton channel (20, 39–41).

In summary, we show that profound acidification occurs at the moment of phagocytotic engulfment, a phenomenon not previously detected. The voltage-gated proton channel responds first during the respiratory burst, rather than Na^+/H^+ antiport as has been believed since 1980 (1). Both Na^+/H^+ antiport and proton channels contribute to pH_i recovery. These findings establish a second crucial role of proton channels during the respiratory burst. It is generally agreed that proton channels compensate the electrogenic activity of the NADPH oxidase, thereby enabling sustained enzyme activity (17, 31–36, 42). That proton channels simultaneously prevent acidification to pH_i low enough to inhibit NADPH oxidase was unexpected.

Materials and Methods

Materials. Dimethyl amiloride, bafilomycin, nigericin, diphenylene iodonium, and zymosan were obtained from Sigma Chemical Co. Di-8-ANEPPS was obtained from Invitrogen.

Neutrophil Isolation. Neutrophils were isolated by density gradient centrifugation (19) from freshly drawn venous blood from healthy adult donors according to a protocol approved by the Institutional Review Board of Rush University Medical Center and consistent with federal regulations. A second

tube of blood drawn specifically for serum preparation was set aside at room temperature for 45 min to coagulate. Blood for neutrophil isolation was diluted 2:1 in PBS/EDTA and layered onto lymphocyte separation medium (LSM) in a 50-mL Falcon centrifuge tube. The tube was centrifuged at 400 × g for 30 min at room temperature. The supernatant, cells at the interface, and excess LSM were aspirated and discarded, leaving the red blood cell and granulocyte pellet. Red cells were removed by hypotonic lysis by adding ice-cold distilled water to the pellet. Adding an equal volume of 2× Hanks' balanced salt solution (HBSS) stopped the lysis. The resulting solution was centrifuged at 400 × g for 10 min at 4 °C. Osmotic shock was repeated 2–3 times depending on the success of the red cell removal. Neutrophils were resuspended in Ringer's solution at 1–2 × 10^{-6} cells per mL and kept on ice until needed.

HVCN1-Deficient Mice. The mouse strain used in this study is B6; 129P2−Hvcn1$^{Gt(RRN293)Byg}$/Mmcd, identification no. 15990-UCD, obtained from the Mutant Mouse Regional Resource Center, a National Center for Research Resources/National Institutes of Health-funded strain repository, and donated to the MMRRC by the National Heart, Blood and Lung Institute-funded BayGenomics project. As in other studies (32, 33), the exogenous gene trap vector sequence, containing an in-frame splice acceptor site followed by coding sequence for a β-galactosidase/neomycin (β-Geo) fusion protein, was inserted into a large intron of 17 kB at ≈12 kB, after exon 2, which contains the first translation initiation codon. Chimaeric male mice were derived from sequence-verified RRN293 genetrap ES cells and used to establish heterozygous wt/RRN293 founders; homozygous offspring were generated from heterozygous mating pairs. Experiments were carried out on 10-wk-old male mice with 129-C57/BL6 mixed background and mice backcrossed with C57/BL6 for 5 generations. Experimental procedures and husbandry were carried out according to the regulations of the United Kingdom's Home Office Animals (Scientific Procedures) Act 1986, prior to Home Office approval.

Mouse Bone Marrow Phagocytes. The hind legs from wild-type and HVCN1 gene trap mice were removed and the femur and tibia freed from surrounding soft tissue. Bones were soaked in 70% ethanol for 1 min. The ends of the bones were cut off and the bone marrow was flushed out with Hank's buffer containing 10% FCS using a 25 G needle and 2 mL syringe. Cells were decanted into a 50-mL tube, leaving debris behind, then washed twice by centrifugation at 200 × g for 8 min. Pelleted cells were resuspended in warm FCS with 10% DMSO and allowed to cool slowly to −80 °C. Frozen cells were shipped on dry ice overnight, then thawed and used immediately.

Zymosan Opsonization. Twenty to 40 mg of zymosan was boiled in ≈25 mL sterile distilled water for 5 min. The solution was allowed to cool, and 25 mL of ice-cold NaCl solution (0.9% wt/vol) was added. The mixture was centrifuged at 400 × g for 10 min at 4 °C. The pellet was then resuspended in 50 mL of ice-cold NaCl and centrifuged again. For human cells, the serum tube was shaken to dislodge the clot and centrifuged at 4 °C. The serum was pipetted off and centrifuged to pellet any residual red cells. Mouse serum was obtained from Sigma. The serum was then added to the washed zymosan at a ratio of 1 mL serum to 20 mg zymosan. The serum/zymosan mixture was then incubated at 37 °C for 1 h. The zymosan pellet was then washed twice with ice-cold PBS (400 × g for 10 min, 4 °C) and resuspended at a concentration of 200 mg/mL.

Dye Loading. A stock solution of SNARF-1 was prepared in ethanol at a concentration of 50 μM and kept at −20 °C. Cells were loaded with a final concentration of 5 μM SNARF-1 by adding 5 μL stock to 50 μL of cell suspension. The suspension was pipetted onto a coverslip and kept at room temperature for 15 min. The coverslip was then placed in the perfusion bath and washed with 3–6 mL of Ringer's solution (at room temperature) to remove excess dye and nonadherent cells. Cells were allowed to stabilize for 15–30 min.

Confocal Microscopy. Cells were visualized using the SEER technique (9) adapted for SNARF-1 (10). This technique requires the simultaneous acquisition of 2 confocal images that are produced by alternating line by line (line interweaving) of 2 excitation wavelengths (543 nm and 594 nm) and 2 emission ranges (550–604 nm and 620–715 nm). The experiments were performed on a Leica TCS SP2 confocal system (Leica Microsystems). The excitation is switched via acousto-optical tunable filters and beam splitters, and the detection wavelengths are determined spectrally. Cells were imaged using a 40× water-immersion lens and scanned at 200 Hz.

The field was chosen with adequately spaced cells so that individual neutrophils could be isolated during the analysis. Neutrophils often migrated extensively during the experiment. Another selection criterion was to avoid

spread neutrophils that often flattened below the confocal plane, which was positioned approximately at the broadest part of the cells. Drugs were added to the bath directly or by complete bath solution exchange. Occasionally cells were washed with Ringer's solution as a control. Cells were pretreated with inhibitors ≈5 min before the addition of 0.1–5 mg/mL OPZ to the bath with gentle trituration. Images were taken every 10–30 s for the remainder of the experiment. Experiments were performed at room temperature.

SNARF-1 Calibration. [H$^+$] was determined from the ratio:

$$[H^+] = \gamma K_d (R - R_{min})/(R_{max} - R) \qquad [1]$$

where γK_d, R_{min}, and R_{max} are defined in Launikonis et al. (9). R_{min} and R_{max} are the ratio R at pH 4.5 and 9.0, respectively. γK_d was obtained by fitting R vs. pH data with Eq. **1** and was 1.1 ± 0.3 μM (mean ± SEM, $n = 4$). Calibration of SNARF-1 was performed by the nigericin/high K$^+$ technique (43). Briefly, cells were washed with high K$^+$ solutions (80–120 mM K$^+$) at different pH con-

taining 10 μM nigericin. The pH$_i$ was allowed to equilibrate with each external solution until the ratio of SNARF-1 no longer changed with time.

Analysis was performed using Leica Lite software (Leica Microsystems) or locally written programs on IDL 6.1 software (ITT Visual Information Solutions).

Electrophysiology. Perforated patch-clamp studies were described in ref. 30.

Statistics. Group means were compared by Student's *t* test.

1. Molski TFP, Naccache PH, Volpi M, Wolpert LM, Sha'afi RI (1980) Specific modulation of the intracellular pH of rabbit neutrophils by chemotactic factors. *Biochem Biophys Res Commun* 94:508–514.
2. Simchowitz L (1985) Chemotactic factor-induced activation of Na$^+$/H$^+$ exchange in human neutrophils. II. Intracellular pH changes. *J Biol Chem* 260:13248–13255.
3. Grinstein S, Furuya W (1986) Cytoplasmic pH regulation in phorbol ester-activated human neutrophils. *Am J Physiol Cell Physiol* 251:C55–C65.
4. Weisman SJ, Punzo A, Ford C, Sha'afi RI (1987) Intracellular pH changes during neutrophil activation: Na$^+$/H$^+$ antiport. *J Leukoc Biol* 41:25–32.
5. Fukushima T, et al. (1996) Na$^+$/H$^+$ exchange activity during phagocytosis in human neutrophils: Role of Fcγ receptors and tyrosine kinases. *J Cell Biol* 132:1037–1052.
6. Jankowski A, Grinstein S (2002) Modulation of the cytosolic and phagosomal pH by the NADPH oxidase. *Antioxid Redox Signal* 4:61–68.
7. Hayashi H, et al. (2008) Na$^+$/H$^+$ exchange and pH regulation in the control of neutrophil chemokinesis and chemotaxis. *Am J Physiol Cell Physiol* 294:C526–C534.
8. Coakley RJ, Taggart C, McElvaney NG, O'Neill SJ (2002) Cytosolic pH and the inflammatory microenvironment modulate cell death in human neutrophils after phagocytosis. *Blood* 100:3383–3391.
9. Launikonis BS, et al. (2005) Confocal imaging of [Ca^{2+}] in cellular organelles by SEER, shifted excitation and emission ratioing of fluorescence. *J Physiol* 567:523–543.
10. Musset B, et al. (2008) A pH-stabilizing role of voltage-gated proton channels in IgE-mediated activation of human basophils. *Proc Natl Acad Sci USA* 105:11020–11025.
11. Demaurex N, Downey GP, Waddell TK, Grinstein S (1996) Intracellular pH regulation during spreading of human neutrophils. *J Cell Biol* 133:1391–1402.
12. Gottlieb RA, Giesing HA, Zhu JY, Engler RL, Babior BM (1995) Cell acidification in apoptosis: Granulocyte colony-stimulating factor delays programmed cell death in neutrophils by up-regulating the vacuolar H$^+$-ATPase. *Proc Natl Acad Sci USA* 92:5965–5968.
13. Weiss SJ, Klein R, Slivka A, Wei M (1982) Chlorination of taurine by human neutrophils. Evidence for hypochlorous acid generation. *J Clin Invest* 70:598–607.
14. Foote CS, Goyne TE, Lehrer RI (1983) Assessment of chlorination by human neutrophils. *Nature* 301:715–716.
15. Thomas EL, Grisham MB, Jefferson MM (1983) Myeloperoxidase-dependent effect of amines on functions of isolated neutrophils. *J Clin Invest* 72:441–454.
16. Chapman ALP, Hampton MB, Senthilmohan R, Winterbourn CC, Kettle AJ (2002) Chlorination of bacterial and neutrophil proteins during phagocytosis and killing of Staphylococcus aureus. *J Biol Chem* 277:9757–9762.
17. Murphy R, DeCoursey TE (2006) Charge compensation in phagocytes. *Biochim Biophys Acta* 1757:996–1011.
18. Kettle AJ, Gedye CA, Hampton MB, Winterbourn CC (1995) Inhibition of myeloperoxidase by benzoic acid hydrazides. *Biochem J* 308:559–563.
19. DeCoursey TE, Cherny VV, Zhou W, Thomas LL (2000) Simultaneous activation of NADPH oxidase-related proton and electron currents in human neutrophils. *Proc Natl Acad Sci USA* 97:6885–6889.
20. DeCoursey TE (2003) Voltage-gated proton channels and other proton transfer pathways. *Physiol Rev* 83:475–579.
21. Nanda A, et al. (1996) Activation of proton pumping in human neutrophils occurs by exocytosis of vesicles bearing vacuolar-type H$^+$-ATPases. *J Biol Chem* 271:15963–15970.
22. DeCoursey TE, Cherny VV (1994) Voltage-activated hydrogen ion currents. *J Membr Biol* 141:203–223.
23. DeCoursey TE, Ligeti E (2005) Regulation and termination of NADPH oxidase activity. *Cell Mol Life Sci* 62:2173–2193.

24. Li XJ, et al. (2009) A fluorescently tagged C-terminal fragment of p47^{phox} detects NADPH oxidase dynamics during phagocytosis. *Mol Biol Cell* 20:1520–1532.
25. Reeves EP, et al. (2002) Killing activity of neutrophils is mediated through activation of proteases by K$^+$ flux. *Nature* 416:291–297.
26. Hampton MB, Kettle AJ, Winterbourn CC (1996) Involvement of superoxide and myeloperoxidase in oxygen-dependent killing of Staphylococcus aureus by neutrophils. *Infect Immun* 64:3512–3517.
27. Hampton MB, Kettle AJ, Winterbourn CC (1998) Inside the neutrophil phagosome: Oxidants, myeloperoxidase, and bacterial killing. *Blood* 92:3007–3017.
28. Painter RG, Wang G (2006) Direct measurement of free chloride concentrations in the phagolysosomes of human neutrophils. *Anal Chem* 78:3133–3137.
29. Moreland JG, Davis AP, Bailey G, Nauseef WM, Lamb FS (2006) Anion channels, including ClC-3, are required for normal neutrophil oxidative function, phagocytosis, and transendothelial migration. *J Biol Chem* 281:12277–12288.
30. Morgan D, Cherny VV, Murphy R, Katz BZ, DeCoursey TE (2005) The pH dependence of NADPH oxidase in human eosinophils. *J Physiol* 569:419–431.
31. Capasso M, et al. (2008) The voltage-gated proton channel HVCN1 co-localizes with B cell receptor and is involved in class switch recombination in vivo. *Blood ASH Meeting Abstracts* 112:707.
32. Ramsey IS, Ruchti E, Kaczmarek JS, Clapham DE (2009) Hv1 proton channels are required for high-level NADPH oxidase-dependent superoxide production during the phagocyte respiratory burst. *Proc Natl Acad Sci USA* 106:7642–7647.
33. Okochi Y, Sasaki M, Iwasaki H, Okamura Y (2009) Voltage-gated proton channel is expressed on phagosomes. *Biochem Biophys Res Commun* 382:274–279.
34. Henderson LM, Chappell JB, Jones OTG (1987) The superoxide-generating NADPH oxidase of human neutrophils is electrogenic and associated with an H$^+$ channel. *Biochem J* 246:325–329.
35. Bánfi B, et al. (1999) A novel H$^+$ conductance in eosinophils: Unique characteristics and absence in chronic granulomatous disease. *J Exp Med* 190:183–194.
36. DeCoursey TE, Morgan D, Cherny VV (2003) The voltage dependence of NADPH oxidase reveals why phagocytes need proton channels. *Nature* 422:531–534.
37. van Zwieten R, Wever R, Hamers MN, Weening RS, Roos D (1981) Extracellular proton release by stimulated neutrophils. *J Clin Invest* 68:310–313.
38. Borregaard N, Schwartz JH, Tauber AI (1984) Proton secretion by stimulated neutrophils: Significance of hexose monophosphate shunt activity as source of electrons and protons for the respiratory burst. *J Clin Invest* 74:455–459.
39. Morgan D, Cherny VV, Price MO, Dinauer MC, DeCoursey TE (2002) Absence of proton channels in COS-7 cells expressing functional NADPH oxidase components. *J Gen Physiol* 119:571–580.
40. Henderson LM, Banting G, Chappell JB (1995) The arachidonate-activatable, NADPH oxidase-associated H$^+$ channel. Evidence that gp91-phox functions as an essential part of the channel. *J Biol Chem* 270:5909–5916.
41. Bánfi B, et al. (2000) A mammalian H$^+$ channel generated through alternative splicing of the NADPH oxidase homolog NOH-1. *Science* 287:138–142.
42. Femling JK, et al. (2006) The antibacterial activity of human neutrophils and eosinophils requires proton channels but not BK channels. *J Gen Physiol* 127:659–672.
43. Thomas JA, Buchsbaum RN, Zimniak A, Racker E (1979) Intracellular pH measurements in Ehrlich ascites tumor cells utilizing spectroscopic probes generated in situ. *Biochemistry* 18:2210–2218.

PHYSIOLOGY